Hindawi
Mathematical Problems in Engineering
Volume 2018, Article ID 3208934, 16 pages
https://doi.org/10.1155/2018/3208934

Research Article

A Multiobjective Scheduling Optimization Model for Multienergy Complementary System Integrated by Wind-Photovoltaic-Convention Gas Turbines considering Demand Response

Zhang Lihui,[1] Xin He,[1] and Ju Liwei [2,3]

[1]*North China Electric Power University, Beijing 102206, China*
[2]*Academy of Chinese Energy Strategy, China University of Petroleum-Beijing, Beijing 102249, China*
[3]*Beijing Energy Development Research Base, Beijing 102206, China*

Correspondence should be addressed to Ju Liwei; 183758841@qq.com

Received 14 May 2018; Accepted 10 July 2018; Published 31 July 2018

Academic Editor: Anna Vila

To utilize the complementary feature of different power sources, wind power plant (WPP), and solar photovoltaic power (PV), convention gas turbines (CGT) and incentive-based demand response (IBDR) are integrated into a multienergy complementary system (MECS) with the implementation of price-based demand response (PBDR). Firstly, the power output model of WPP, PV, and CGT is constructed and the mathematical model of DR is presented. Then, a multiobjective scheduling model is proposed for MECS operation under the objective functions of the maximum economic benefit, the minimum abandoned energy, and the minimum risk level. Thirdly, the payoff table of objective functions is put forward for converting the multiobjective model into a single objective model by using entropy weight method to calculate weighting coefficients of different objective functions. Finally, the improved IEEE 30 bus system is taken as the simulation system with four simulation scenarios for comparatively analyzing the influence of PBDR and IBDR on MECS operation. The simulation results show the following: (1) The MECS fully utilized the complementarity of different power sources; CGT and IBDR can provide peaking service for WPP and PV to optimize overall system operation. (2) The proposed algorithm can solve the MECS multiobjective scheduling optimization model, and the system scheduling results in the comprehensive optimal mode can take into account different appeal. And the total revenue, abandoned energy capacity, and load fluctuation are, respectively, 108009.30¥, 11.62 MW h, and 9.74 MW. (3) PBDR and IBDR have significant synergistic optimization effects, which can promote the grid connection of WPP and PV. When they are both introduced, the peak-to-valley ratio of the load curve is 1.19, and the abandoned energy is 5.85 MW h. Therefore, the proposed MECS scheduling model and solution algorithm could provide the decision basis for decision makers based on their actual situation.

1. Introduction

The consumption structure dominated by fossil energy in China has led to the severe environmental problems in economic growth. To solve the increasingly significant contradiction between energy, economy, and environment, clean energy power generation, especially wind power and photovoltaic power, has attracted worldwide attention. The development speed and scale of clean energy power generation are increasing year by year. By the end of 2017, China's cumulative wind power and photovoltaic installed capacity reached 164 GW and 130 GW, and the generation capacity of wind power and photovoltaic power has reached 305.7 billion kW h and 118.2 billion kW h. However, due to the randomness and volatility of wind power and photovoltaic power, the abandoned energy problem is increasingly serious. In 2017, the wind and photovoltaic abandoned power generation was 36.684 billion kW h and 10.92 billion kW h, respectively [1]. To solve the above problems, it is necessary to match sufficient auxiliary power sources for wind power and photovoltaic

power, which has important theoretical value and practical significance for solving the wind and photovoltaic abandoned power generation.

In general, the auxiliary power sources for clean energy generation mainly include conventional coal-fired generator sets and Energy Storage System (ESS). For coal-fired generator sets, due to the pollutant emissions from power generation, the applicability will gradually be replaced by convention gas turbines (CGT) [2]. As for ESS, the linkage optimization goal between user side and generation side is achieved by its charging-discharging characteristics. Therefore, ESS could be regarded as one of the important auxiliary power sources for the grid connection of wind power and photovoltaic power. However, because ESS technology is still not mature enough, the high ESS's cost leads to great difficulties in its promotion [3]. In recent years, with the rapid development of smart grid, advanced intelligent management means, information interaction systems, and power electronics technology have provided a path to guide the terminal customer to respond to system scheduling. Demand response (DR) has changed the original power source by tracking load scheduling method. DR can fully incentivize distributed resources in user side to participate in system scheduling and provide a new research idea for clean energy generation [4]. Therefore, designing optimized operation strategies for wind power, photovoltaic power, CGT, and DR has important theoretical and practical significance for solving the contradictions between economy, energy, and environment.

From the perspective of operating characteristics, the coupled operation of WPP, PV, CGT, and DR presents the characteristics of "source-network-load" interaction and could realize the optimized configuration of various resources in a diversified energy system space, namely, the multienergy complementary system (MECS) [5]. For the above types of MECS, domestic and foreign scholars focus on the three aspects: capacity optimization configuration, scheduling operation strategy, and mathematical model solution. In terms of capacity configuration, it is mainly to make full use of the complementarity between different energy sources, rationally allocating the capacity proportion of clean energy power generation to increase the grid connection of clean energy generation. Ding et al. [6] established an independent wind-photovoltaic-diesel-storage microgrid system with the objective of maximum comprehensive cost. Zhu et al. [7] proposed a battery capacity determination method based on battery internal characteristics from the perspective of continuous power supply of independent wind-photovoltaic-storage microgrid system. Georgios et al. [8] presented a novel methodological framework for the investigation of uncertainty in the context of DES design, which combines optimization-based DES models and techniques with Uncertainty Analysis (UA) and Global Sensitivity Analysis (GSA). Liu et al. [9] aimed at minimizing the annual investment replacement cost, operation-maintenance cost, and controllable load scheduling cost and established an independent microgrid capacity configuration optimization model considering controllable load. From the above literatures, it can be seen that the existing research results have conducted in-depth research on the capacity allocation of MECS and have been verified in practice.

In terms of operation strategy, it is mainly to select the reasonable operation objective and construct the operation optimization mechanism based on system internal and external resource conditions. Aboelsood et al. [10] presented an optimal deployment with respect to capacity sizes and types of DG (distributed generation) for CHP (combined heat and power) systems within microgrids. Xu et al. [11] selected the maximum economic benefit as the optimization objective and established an independent MECS simulation system under different operation strategies. Huang et al. [12] proposed the optimal operation mode of MECS based on the objective of minimum total cost including investment operation cost and energy shortage cost. Hrvoje et al. [13] considered a weekly self-scheduling of a virtual power plant composed of intermittent renewable sources, storage system, and a conventional power plant. Duan et al. [14] introduced the capital yield index considering risk adjustment to establish a balanced relationship between benefits and risk. Mohammad et al. [15] proposed a virtual power plant integrated by DG, ESS, and controllable loads under the objective of the minimum total operation cost considering energy loss cost. Zhu et al. [16] established the scheduling models of the power grid, power source, and load layers considering the influence of various uncertainties, respectively, to realize the complementary feature of power source and active load.

In terms of mathematical model solution, MECS operation should balance operation appeal in multiple aspects since it involves multiple energy entities. Correspondingly, the optimization operation model for MECS is also a multiobjective model. Therefore, how to convert or solve the multiobjective model is the key problem to determine the optimal operation strategy. The multiobjective model has the characteristics of multivariables, multiobjectives, and nonlinearity, which requires the corresponding algorithm to obtain the optimized result. The solution algorithm is mainly divided into traditional algorithm [17] and heuristic intelligent algorithm [18]. Soltani et al. [19] employed a lexicographic optimization in combination with hybrid augmented-weighted ε-constraint method to obtain Pareto optimal solutions of the multiobjective unit commitment problem and applied a fuzzy decision-making to select the most preferred nondominated solution. Wang et al. [20] combined the chaos optimization algorithm with the multiobjective genetic algorithm and proposed a chaotic multiobjective genetic algorithm to optimize the system capacity of the independent microgrid. Mohsen et al. [21] developed an improved real-coded genetic algorithm and an enhanced mixed integer linear programming (MILP) based method to schedule the unit commitment and economic dispatch of microgrid units. Chen et al. [22] proposed a fuzzy multiobjective hybrid particle swarm optimization (PSO) model based on chance constrained programming and introduced fuzzy global optimal solution and synchronous particle local search to improve search efficiency.

The optimization problem for MECS operation has been extensively discussed in all aforementioned studies. The capacity allocation method, operation optimization model, and model solution algorithm for MECS operation have been proposed which could greatly promote the development.

However, it should be noted that there are some insufficiencies on the optimization of MECS operation. Firstly, the existing research results have discussed the capacity configuration of WPP, PV, and CGT but failed to consider the impact of DR on system capacity configuration. In fact, DR can invoke user side resources to system operation and affect the system optimization operation strategy. Then, with regard to the selection of operation objectives, the existing literatures mainly select the minimum cost or maximum return as the objective function but ignore the clean energy generation characteristics. Clean energy has environment-friendly features; thus the minimum abandoned clean energy can give full play to its environmental benefits. However, the output volatility of clean energy will also bring significant risks. How to balance the relationships between economy, environment, and risk is crucial for establishing the optimal operation strategy. Finally, although the heuristic optimization algorithm can obtain an optimal solution set, when the selection of individual extremum does not meet the multiobjective planning principle, the algorithm is easily trapped into a local extremum. Besides, the algorithm has high complexity and is difficult to put into practice. Therefore, how to convert the multiobjective model into a single objective model and then solve the model is the key guarantee for establishing MECS operation strategy. All above analysis motivates us to put forward a risk aversion scheduling model for MECS. The main contributions of this work are summarized as follows:

(i) WPP, PV, CGT, and IBDR are integrated into MECS. Firstly, the basic structure of MECS is proposed, and the function of different components is defined. Then, the power output model of WPP and PV is constructed based on the probability distribution function. Finally, the mathematical model of price-based demand response (PBDR) and incentive-based demand response (IBDR) is constructed for motivating terminal users to participate in the optimal scheduling in generation side.

(ii) A multiobjective model for MECS is proposed considering the influence of PBDR. Firstly, the mathematical models of WPP, PV, CGT, and DR are constructed. Then, three objective functions of the maximum economic benefit, the minimum abandoned energy, and the minimum risk level are chosen for constructing the scheduling optimization model considering system operation constraint conditions.

(iii) A solving algorithm for multiobjective model is proposed. Firstly, the optimal scheduling strategy under each single objective optimization mode is calculated, and the payoff table of objective function is established. Secondly, the decreasing half gradient membership function and ascending half line membership function are used to process the objective function, and the entropy weight method is used to obtain weight coefficient of the objective function. Then, according to the weight coefficient of objective function, a comprehensive single objective optimization model is formed. Finally, four scenarios are set for comparative analysis and the improved IEEE30 bus system is taken as simulation system.

The rest of this paper is organized as follows: Section 2 describes the basic structure of MECS, constructs the power output model of WPP, PV, and CGT, and presents the demand response models including the PBDR model and IBDR model. Section 3 constructs the multiobjective functions for MECS optimization scheduling under the objective of the maximum economic benefit, the minimum abandoned energy, and the minimum risk level considering system operation constraint conditions. Then, in order to solve the proposed model, Section 4 puts forward a solution algorithm for multiobjective model based on the payoff table of single objective optimization model and entropy weight method. Section 5 chooses the improved IEEE30 bus system as simulation system, and four scenarios are set for comparative analysis. Section 6 highlights the contributions and conclusions of the paper.

2. MECS Describe

2.1. MECS Composition. In the paper, MECS is integrated by WPP, PV, CGT, and IBDRs. WPP and PV are mainly used to meet the load demand. When WPP and PV have difficulty meeting the load demand, CGT is used to meet the surplus load. Simultaneously, CGT can also provide reserve service for WPP and PV. In addition, IBDR can provide power output by aggregating user side load. When power output is positive, IBDR belongs to the power supply side. Conversely, when power output is negative, IBDR belongs to the user side. At the same time, in order to make full use of the user side load resources, PBDR is implemented. Through implementing time-of-use (TOU) price, PBDR can optimize consumer consumption behavior, realize peak load shifting, and provide greater grid-connected capacity for WPP and PV. Figure 1 shows the basic structure of MECS.

2.2. Power Source Output Model. In the proposed MECS, power source mainly includes WPP, PV, and CGT. The section mainly introduces output models of WPP and PV.

2.2.1. WPP Output Model. For wind turbines, the output power mainly depends on the natural wind speed. Due to the random feature of natural wind, WPP output power has random characteristics. In order to describe the WPP output, the Rayleigh distribution function is generally used to describe the wind speed distribution [2]. The specific calculation is shown in

$$f(v) = \frac{\varphi}{\vartheta}\left(\frac{v}{\vartheta}\right)^{\varphi-1} e^{-(v/\vartheta)^{\varphi}} \tag{1}$$

wherein v represents real-time wind speed. φ,ϑ represent shape parameter and scale parameter. Eq. (1) is used to obtain the expected value and variance of wind speed distribution. On the basis, the following equations can be used to calculate the real-time WPP output power:

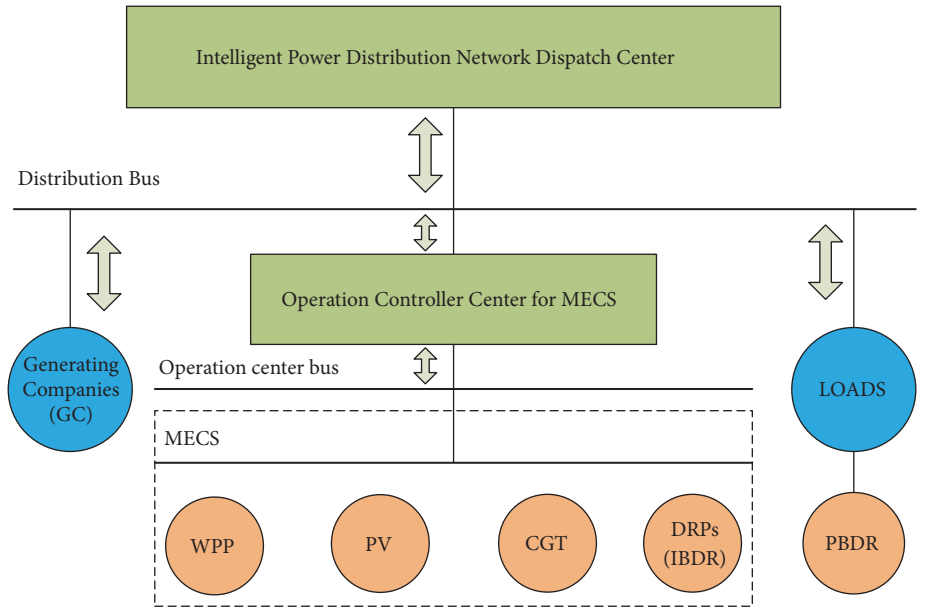

Figure 1: The basic structure of MECS.

$$g^*_{W,t} = \begin{cases} 0, & 0 \le v_t < v_{in},\ v_t > v_{out} \\ \dfrac{v_t - v_{in}}{v_{rated} - v_{in}} g_R, & v_{in} \le v_t \le v_{rated} \\ g_R, & v_{rated} \le v_t \le v_{out} \end{cases} \tag{2}$$

$$0 \le g_{W,t} \le g^*_{W,t} \tag{3}$$

wherein v_t represents WPP real-time wind speed at time t. v_{in}, v_{rated}, and v_{out} represent cut-in, rated, and cut-out wind speed.

2.2.2. PV Output Model. For photovoltaic generators, the output power mainly depends on the solar radiation intensity. The literature [4] proves that the Beta distribution function can be used to describe the solar photovoltaic radiation intensity, and the specific calculation is as follows:

$$f(\theta) = \begin{cases} \dfrac{\Gamma(\alpha)\Gamma(\beta)}{\Gamma(\alpha)+\Gamma(\beta)} \theta^{\alpha-1}(1-\theta)^{\beta-1}, & 0 \le \theta \le 1,\ \alpha \ge 0,\ \beta \ge 0 \\ 0, & otherwise \end{cases} \tag{4}$$

wherein θ represents the PV radiation intensity. α and β represent the shape parameter of the Beta distribution. After obtaining the expected value and variance of the PV radiation intensity, α and β can be calculated by

$$\beta = (1-\mu) \times \left(\frac{u \times (1-\mu)}{\sigma^2} - 1 \right) \tag{5}$$

$$\alpha = \mu \left[\frac{\mu(1-\mu)}{\sigma^2} - 1 \right] \tag{6}$$

wherein u and σ represent the expected value and standard deviation of PV radiation intensity, respectively. Substituting (5)-(6) into (4) can obtain the PV radiation intensity distribution function. Then, based on the photoelectric conversion equation, the PV output at time t can be calculated:

$$g^*_{PV,t} = \eta_{PV} \times S_{PV} \times \theta_t \tag{7}$$

$$0 \le g_{PV,t} \le g^*_{PV,t} \tag{8}$$

wherein η_{PV} and S_{PV} represent the radiation area and radiation efficiency. θ_t represents the radiation intensity at time t.

2.3. DR Mathematical Model

2.3.1. PBDR Model. DR is mainly divided into PBDR and IBDR. PBDR mainly guides the rational use of electricity by formulating diversified electricity price mechanisms and responds to system scheduling demands. According to the demand-side correlation principle of microeconomics, PBDR is mainly described by the demand elasticity coefficient, and the electricity price elasticity is defined as follows:

$$e_{st} = \frac{\Delta L_s / L^0_s}{\Delta P_t / P^0_t} \quad \begin{cases} e_{st} \le 0, & s = t \\ e_{st} \ge 0, & s \ne t \end{cases} \tag{9}$$

wherein ΔL_s, ΔP_t, respectively, represent the fluctuation of load demand and price before and after DR.

Based on the concept of demand elasticity coefficient, PBDR mainly implements the TOU strategy to optimize the user electricity consumption behavior, thereby achieving the

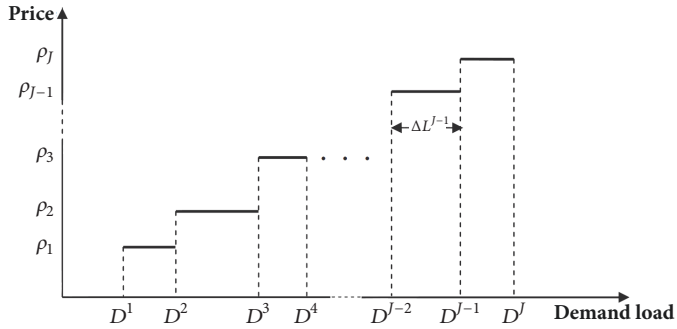

Figure 2: Stepwise DR price-demand curve.

peak load shifting goal in load curve, and the load changes after DR is as follows:

$$L_t = L_t^0 \times \left\{1 + e_{tt} \times \frac{\left[P_t - P_t^0\right]}{P_t^0} + \sum_{\substack{s=1 \\ s \neq t}}^{24} e_{st} \times \frac{\left[P_s - P_s^0\right]}{P_s^0}\right\} \quad (10)$$

wherein L_t^0, L_t and P_t^0, P_t, respectively, represent load demand and price before and after DR. s, t represent time, s, t =1, 2, …, T. e_{st} represents the electricity price, when $s = t$, e_{st} is called for self-elasticity and when $s \neq t$, e_{st} is called for cross elasticity. The specific derivation process is described in literature [5].

$$\Delta L_{PB,t} = L_t - L_t^0 \quad (11)$$

wherein $\Delta L_{PB,t}$ represents the load variation for PBDR at time t.

2.3.2. IBDR Model. IBDR is achieved through signing the DR agreement with the user in advance. When the response demand occurs, the system requests the user to increase or decrease the load demand according to the agreement and provides corresponding response compensation in accordance with the agreement. The specifics are shown in literature [5]. In general, IBDR is mainly provided by demand response providers (DRPs). Since the income of DRPs is determined by DR supply price, DPRs will step by step participate in IBDR according to the volatility of the electricity market price. The corresponding stepwise smart DR price-demand curve is shown in Figure 2.

As shown in Figure 2, the minimum DR for the i-th DRP in step j is $D_i^{j,\min}$; the maximum developable DR is $D_i^{j,\max}$. DRPs can participate in both energy market scheduling and reserve market scheduling. Eq. (12)-(14) describe the load reduction relationship of DRPs participating in energy market:

$$D_i^{j,\min} \leq \Delta L_{i,t}^j \leq D_{i,t}^j, \quad j = 1 \quad (12)$$

$$\left|\Delta L_{i,t}^j\right| \leq \left(D_{i,t}^j - D_{i,t}^{j-1}\right), \quad j = 2, 3, \ldots, J \quad (13)$$

$$\Delta L_{IB,t} = \sum_{i=1}^{I}\sum_{j=1}^{J} \Delta L_{i,t}^j = \Delta L_{IB,t}^+ + \Delta L_{IB,t}^- \quad (14)$$

wherein $\Delta L_{i,t}^j$ represents the load reduction for the i-th DRP at time t in step j. $D_{i,t}^j$ represents the providable load reduction of the i-th DRP at time t in step j. $\Delta L_{i,t}^E$ represents the cumulative load reduction for the i-th DRP at time t. $\Delta L_{IB,t}$ represents output power provided by IBDR at time t. $\Delta L_{IB,t}^+$ represents the positive output power provided by IBDR at time t. $\Delta L_{IB,t}^-$ represents the negative output power provided by IBDR at time t.

3. The Multiobjective Optimization Model for MECS

3.1. Objective Function. MECS includes WPP, PV, and CGT, which has good environmental and economic characteristics. And the coupled operation of multiple energy sources will bring significant economic and environmental benefits. Meanwhile, system needs to consume renewable energy sources such as wind energy and solar energy and minimize the abandoned energy. Therefore, the maximum economic benefit and the minimum abandoned energy should be the optimization operation objectives for MECS. However, due to the randomness and volatility of WPP and PV, the grid connection of clean energy power generation will bring great risks. Therefore, it needs to control the system operation risk level while pursuing maximum economic benefit and the minimum abandoned energy. Therefore, the paper selects the objective functions of the maximum economic benefit, the minimum abandoned energy, and the minimum risk level. The specific objective functions are as follows.

(1) The Maximum Economic Benefit Objective. The economic benefits of MECS include four parts: WPP power generation

benefit, PV power generation benefit, CGT power generation benefit, and DR operation benefit. The specific objective function is as follows:

$$\max f_1 = \sum_{t=1}^{T} \left(R_{W,t} + R_{PV,t} + R_{CGT,t} + R_{DR,t}\right) \tag{15}$$

wherein $R_{W,t}$, $R_{PV,t}$, $R_{CGT,t}$, and $R_{DR,t}$, respectively, represent WPP, PV, CGT, and DR power generation benefits at time t.

$$R_{W,t} = \rho_{W,t} g_{W,t} \tag{16}$$

$$R_{PV,t} = \rho_{PV,t} g_{PV,t} \tag{17}$$

$$R_{CGT,t} = \rho_{CGT,t} g_{CGT,t} - \pi^{pg}_{CGT,t} - \pi^{ss}_{CGT,t} \tag{18}$$

wherein $\pi^{pg}_{CGT,t}$ and $\pi^{ss}_{CGT,t}$ represent the generation cost and startup-shutdown cost of CGT at time t.

$$\pi^{pg}_{CGT,t} = a_{CGT} + b_{CGT} g_{CGT} + c_{CGT} \left(g_{CGT,t}\right)^2 \tag{19}$$

$$\pi^{ss}_{CGT,t} = \left[u_{CGT,t} \left(1 - u_{CGT,t}\right)\right] D_{CGT,t} \tag{20}$$

$$D_{CGT,t} = \begin{cases} N^{hot}_{CGT}, T^{\min}_{CGT} < T^{\text{off}}_{CGT,t} \le T^{\min}_{CGT} + T^{\text{cold}}_{CGT} \\ N^{cold}_{CGT}, T^{\text{off}}_{CGT,t} > T^{\min}_{CGT} + T^{\text{cold}}_{CGT} \end{cases} \tag{21}$$

wherein a_{CGT}, b_{CGT}, and c_{CGT} represent cost coefficient power generation of CGT. g_{CGT} represents the generation power of CGT at time t. $u_{CGT,t}$ is the operation status of CGT at time t, a binary variable. $u_{CGT,t} = 1$ means the CGT is in operation, whereas $u_{CGT,t} = 0$ means CGT is not in operation. $D_{CGT,t}$ represents the startup-shutdown cost of CGT. N^{hot}_{CGT} and N^{cold}_{CGT} represent hot startup cost and cold startup cost of CGT. $T^{\min}_{CGT}$ is the minimum allowable downtime of CGT. $T^{\text{off}}_{CGT,t}$ is the continuous downtime of CGT at time t. T^{cold}_{CGT} is cold startup time of CGT. $T^{\text{off}}_{CGT,t}$ is downtime of CGT.

$$R_{DR,t} = R^{PB}_{DR,t} + R^{IB}_{DR,t} \tag{22}$$

$$R^{PB}_{DR,t} = P_t L_t - P^0_t L^0_t \tag{23}$$

$$R^{IB}_{DR,t} = P^+_{IB,t} \Delta L^+_{IB,t} + \left(P_t - P^-_{IB,t}\right) \Delta L^-_{IB,t} \tag{24}$$

wherein P_t and P^0_t are the price at time t before and after PBDR. $P^+_{IB,t}$ is the positive output power price provided by IBDR at time t. $P^-_{IB,t}$ is the negative output power price provided by IBDR at time t. When IBDR provides negative output power, it indicates that the power consumption is increased and it can enjoy electricity price discount at this time, showing that the revenue is the reduction of electricity cost.

(2) The Minimum Abandoned Energy Objective. There are wind energy and solar energy in MECS. Therefore, the abandoned energy mainly includes abandoned wind and abandoned photovoltaic power. The paper selects the minimum abandoned energy as one of the objective functions. The specific objective function is as follows:

$$\min f_2 = \sum_{t=1}^{T} \left\{\left(g^*_{W,t} - g_{W,t}\right) + \left(g^*_{PV,t} - g_{PV,t}\right)\right\} \tag{25}$$

(3) The Minimum Risk Level Objective. MECS makes full use of wind power and photovoltaic power generation, but its volatility and randomness also bring great risks to system operation. Therefore, the paper selects system net load fluctuation as the risk measure index and set the minimum net load fluctuation as objective function:

$$\min f_3 = \left\{\sum_{t=1}^{T} \frac{\left[g_{W,t} + g_{PV,t} - \left(\Delta L^-_{IB,t} - \Delta L^+_{IB,t}\right) - g_{av}\right]^2}{T}\right\}^{1/2} \tag{26}$$

$$g_{av} = \sum_{t=1}^{T} \frac{\left[g_{W,t} + g_{PV,t} - \left(\Delta L^-_{IB,t} - \Delta L^+_{IB,t}\right)\right]}{T} \tag{27}$$

wherein N represents the standard deviation of WPP and PV output power fluctuations. T is system scheduling cycle. g_{av} represents the average system output power. Therefore, when N is smaller, the output power fluctuation of WPP and PV is lower, which is more beneficial to system safe operation.

3.2. Constraint Conditions. MECS is composed of WPP, PV, and CGT. Therefore, it needs to meet the system supply and demand balance constraint, WPP, PV, and CGT operation constraints, and system spin reserve constraint in operation.

(1) Supply and Demand Balance Constraint

$$\underbrace{g_{W,t}\left(1 - \varphi_W\right) + g_{PV,t}\left(1 - \varphi_{PV}\right) + + g_{CGT,t}\left(1 - \varphi_{CGT}\right) + \mu_{IB,t} \Delta L_{IB,t}}_{MECS\ output} + g_{GC,t} = L_t - \mu_{PB,t} \Delta L_{PB,t} \tag{28}$$

wherein φ_W, φ_{PV}, and φ_{CGT} are power loss rates of WPP, PV, and CGT, respectively. $g_{GC,t}$ is power output of system purchasing from generation company. $\mu_{IB,t}$, $\mu_{PB,t}$, respectively, are IBDR and PBDR state variables, the 0-1 variables, when $\mu_{IB,t}$ or $\mu_{PB,t} = 1$, indicating that the DR is implemented.

(2) CGT Operation Constraints. CGT operation constraints mainly include unit power generation output constraint, unit climbing constraint, and unit startup-shutdown time constraints.

$$u_{CGT,t} g^{\min}_{CGT} \le g_{CGT,t} \le u_{CGT,t} g^{\max}_{CGT} \tag{29}$$

$$u_{CGT,t}\Delta g^{-}_{CGT} \le g_{CGT,t} - g_{CGT,t-1} \le u_{CGT,t}\Delta g^{+}_{CGT} \tag{30}$$

$$\left(T^{\text{on}}_{CGT,t-1} - M^{\text{on}}_{CGT}\right)\left(u_{CGT,t-1} - u_{CGT,t}\right) \ge 0 \tag{31}$$

$$\left(T^{\text{off}}_{CGT,t-1} - M^{\text{off}}_{CGT}\right)\left(u_{CGT,t} - u_{CGT,t-1}\right) \ge 0 \tag{32}$$

wherein $g^{\max}_{CGT}$ and $g^{\min}_{CGT}$ are the upper and lower limitation of CGT generation output, respectively. Δg^{+}_{CGT}, Δg^{-}_{CGT} are the upper and lower limitation of CGT climbing power, respectively. M^{on}_{CGT} and M^{off}_{CGT} are the minimum startup time and the minimum shutdown time of CGT, respectively. $T^{\text{on}}_{CGT,t-1}$ and $T^{\text{off}}_{CGT,t-1}$ are the continuous operation time and the continuous shutdown time of CGT at time t-1, respectively.

(3) DR Constraints. DR constraints include PBDR constraint and IBDR constraint. PBDR can use time-of-use (TOU) price to achieve the peak load shifting goal in load curve. However, it is necessary to control the load fluctuation amplitude so as to avoid "peak-valley upside down" phenomenon. The specific constraints are as follows:

$$\sum_{t=1}^{T}\left|\Delta L_{PB,t}\right| \le \Delta L^{\max}_{PB} \tag{33}$$

$$u_{PB,t}\Delta L^{\min}_{PB,t} \le \Delta L_{PB,t} \le u_{PB,t}\Delta L^{\max}_{PB,t} \tag{34}$$

$$\sum_{t=1}^{T} R^{PB}_{DR,t} \ge 0 \tag{35}$$

wherein $\Delta L^{\max}_{PB}$ is the maximum load variation during the PBDR scheduling period. $\Delta L^{\min}_{PB,t}$ and $\Delta L^{\max}_{PB,t}$ are the upper and lower limitation of load fluctuation of PBDR at time t, respectively. Further, for IBDR, it can aggregate user loads and participate in system scheduling, which can provide positive output and negative output but cannot provide both positive and negative output.

$$u_{IB,t}\Delta L^{\min}_{IB,t} \le \Delta L_{IB,t} \le u_{IB,t}\Delta L^{\max}_{IB,t} \tag{36}$$

$$\Delta L^{+}_{IB,t} \bullet \Delta L^{-}_{IB,t} = 0 \tag{37}$$

wherein $\Delta L^{\min}_{IB,t}$ and $\Delta L^{\max}_{IB,t}$ are the upper and lower limitation of power provided by IBDR at time t, respectively.

(4) Spin Reserve Constraint

$$\begin{aligned}&\left(g^{\max}_{MECS,t} - g_{MECS,t}\right) + \mu_{IB,t}\left(\Delta L^{\max}_{IB,t} - \Delta L_{IB,t}\right)\\ &\quad \ge r_1 \cdot L_t + r_2 \cdot g_{WPP,t} + r_3 \cdot g_{PV,t}\end{aligned} \tag{38}$$

$$\begin{aligned}&\left(g_{MECS,t} - g^{\min}_{MECS,t}\right) + \mu_{IB,t}\left(\Delta L_{IB,t} - \Delta L^{\min}_{IB,t}\right)\\ &\quad \ge r_4 \cdot g_{WPP,t} + r_5 \cdot g_{PV,t}\end{aligned} \tag{39}$$

wherein $g^{\max}_{TPP,t}$ and $g^{\max}_{HS,t}$ are the maximum outputs of TPP and HS at time t. $g^{\min}_{TPP,t}$ and $g^{\min}_{HS,t}$ are the minimum outputs of TPP and HS at time t. r_1, r_2, and r_3 are the upper spin reserve coefficient of load, WPP, and PV. r_4 and r_5 are the lower spin reserve coefficient of WPP and PV.

(5) Other Power Supply Constraints

$$g_{W,t} \le \left(1 - \lambda_{W,t}\right) g^{*}_{W,t} \tag{40}$$

$$g_{PV,t} \le \left(1 - \lambda_{PV,t}\right) g^{*}_{PV,t} \tag{41}$$

wherein $\lambda_{W,t}$ and $\lambda_{PV,t}$ represent the system initiative abandoned wind power at time t. The parameters are mainly based on the system operation status and provide a control tool to decide whether to actively abandon energy.

4. Mathematical Model Solution Algorithm

4.1. Solution Ideas. The coupled system scheduling model constructed in the paper includes multiple optimization objectives and belongs to the multiobjective model. At present, there are two ways to solve the multiobjective model:

(1) Multiobjective model is calculated by intelligent algorithm (such as genetic algorithm, particle swarm algorithm, and ant colony algorithm). Intelligent algorithm can search for optimal solutions in the global scope. But due to the complexity of programming, especially in mathematical model with integer variables, continuous variables, and discrete variables, the solution results may not be perfect.

(2) The weighting function is used to convert the multiobjective model into a single objective model. The objective function weight system can be determined based on the subjective experience of decision-making or mathematical methods.

In the paper, the entropy weight method is used to solve the weight coefficient of the objective function and realize the conversion of the multiobjective model into a single objective model. The calculation steps are as follows: first, the payoff table of system multiobjective scheduling model is calculated. Secondly, based on the payoff table, the paper uses the entropy method to determine the weight coefficient of each target. Thirdly, according to weight coefficients, the multiobjective model is converted into a single objective model.

4.2. Solution Procedure. To convert the multiobjective model into a single objective function, the paper obtains the weights of multiobjective functions by calculating the payoff table. First, the optimal operation strategy of MECS under a single objective function f_i is calculated, and the optimal value f^{*}_{i}, $i = 1, 2, \ldots, I$, is determined. Then, the other objective function values f_{ij} $(i \ne j)$ under the objective function f_i are calculated. Among them, f^{*}_{ii} is the optimal value in f_i. Finally, based on the front calculation results, the payoff table of the objective function can be determined. Table 1 shows the payoff table of the multiobjective functions.

According to the decision attribute table, the decision matrix of the objectives can be obtained as $[f_{ij}]_{I\times I}$ $(i, j = 1, 2, \ldots, I)$. Because the magnitude of the objective functions is different, how to be dimensionalized becomes the key to balance consider each objective function and the weighted integrated objective function. Fuzzy satisfaction theory can

Table 1: the payoff table of the multiobjective functions.

Objective functions	f_1^*	f_2^*	$\cdots$	f_I^*
f_1	f_{11}	f_{12}	$\cdots$	f_{1I}
f_2	f_{21}	$\ddots$	$\cdots$	$\vdots$
$\vdots$	$\vdots$	$\vdots$	$\ddots$	$\vdots$
f_I	f_{I1}	f_{I2}	$\cdots$	f_{II}

effectively reflect the optimization degree of the objective function. However, the objective functions include two optimization directions: the maximum direction and the minimum direction. Therefore, the paper introduces decreasing half gradient membership function and ascending half line membership function to handle the objective function [23]. The specifics are as follows.

When the optimization direction of the objective function is the minimal direction:

$$f_{ij} = \begin{cases} 0, & f_{ij} \geq f_{ij}^{\max},\ j = 1, 2, \ldots, I \\ \dfrac{f_{ij}^{\max} - f_{ij}}{f_{ij}^{\max} - f_{ij}^{\min}}, & f_{ij}^{\min} < f_{ij} < f_{ij}^{\max}\ \&\ j = 1, 2, \ldots, I \\ 1, & f_{ij} \leq f_{ij}^{\min},\ j = 1, 2, \ldots, I \end{cases} \tag{42}$$

When the optimization direction of the objective function is the maximum direction:

$$f'_{ij} = \begin{cases} 1, & f_{ij} \geq f_{ij}^{\max},\ j = 1, 2, \ldots, I \\ \dfrac{f_{ij} - f_{ij}^{\min}}{f_{ij}^{\max} - f_{ij}^{\min}}, & f_{ij}^{\min} < f_{ij} < f_{ij}^{\max}\ \&\ j = 1, 2, \ldots, I \\ 0, & r_{ij} \leq r_{ij}^{\min},\ j = 1, 2, \ldots, I \end{cases} \tag{43}$$

wherein $f_{ij}^{\min}$ and $f_{ij}^{\max}$ are the minimum and maximum values of $f_{ij}(\cdot)$. f'_{ij} is the membership function of $f_{ij}(\cdot)$. According to (37)-(38), the decision matrix after the prehandle $[f'_{ij}]_{k\times k}$can be obtained. Then, the entropy weight method is introduced to solve the weights of the objectives [24]:

(i) Calculate the entropy E_i of objective f_i:

$$E_i = -\psi \sum_{j=1}^{n} f'_{ij} \ln\left(f'_{ij}\right), \quad i = 1, 2, \ldots, I \tag{44}$$

wherein $\psi = 1/\ln(n)$ is a constant related to the sample number, to make $E_i \in [0, 1]$, f'_{ij} satisfies $0 < r'_{ij} < 1$ and $\sum_{j=1}^{n} f'_{ij} = 1$, and when $f'_{ij} = 0$, $f'_{ij} \ln(f'_{ij}) = 0$.

(ii) Calculate the weights of the objective functions:

$$d_i = 1 - E_i, \quad i = 1, 2, \ldots, k \tag{45}$$

$$\lambda_i = \frac{d_i}{\sum_{i=1}^{i} d_i}, \quad i = 1, 2, \ldots, k \tag{46}$$

Then, the weights of the single objectives with their weight coefficients are used to synthesize the objective function as follows:

$$\overline{F} = \min \left\{ \sum_{i' \in i} \lambda_{i'} \frac{\max_{i'} \left\{f^*_{i'j}\right\} - f_{i'}}{\max_{i'} \left\{f^*_{i'j}\right\} - \min_{i'} \left\{f^*_{i'j}\right\}} + \sum_{i'' \in i, i'' \neq i'} \lambda_{i''} \frac{f_{i''} - \min_{i''} \left\{f^*_{i''j}\right\}}{\max_{i''} \left\{f^*_{i''j}\right\} - \min_{i''} \left\{f^*_{i''j}\right\}} \right\}, \quad \left\{i'\right\} \cup \left\{i''\right\} = \{i\} \tag{47}$$

wherein $\lambda_{i'}$ and $\lambda_{i''}$ are the weight coefficients of the minimum and maximum objective function. The weighted integrated objective function $\overline{F}$ can be obtained by (47). Combining (28)-(41), MECS scheduling optimal satisfactory solution, which takes into account each objective function, can be solved.

5. Simulation Analysis

5.1. Scenario Setting. To analyze the optimization effects of PBDR and IBDR on MECS operation, this section divides four simulation scenarios for comparative analysis. The specific scenarios are set as follows.

Case 1 (basic scenario). Self-scheduling of MECS without PBDR and IBDR: The scenario is mainly used to verify the validity of the multiobjective model solution algorithm and to analyze the complementary effects among WPP, PV, and CGT.

Case 2 (PBDR scenario). Self-scheduling of MECS only with PBDR: The scenario is mainly used to analyze the optimization effect of PBDR on MECS operation. Through contrasting with Case 1, the influences of PBDR on the smoothness of the load demand curve and on the enhancing effect of the grid connection capacity of WPP and PV are analyzed.

Case 3 (IBDR scenario). Self-scheduling of MECS only with IBDR: The scenario is mainly used to analyze the optimization effect of IBDR on MECS operation. Through contrasting with Case 1, the reserve effects of IBDR on the grid connection of WPP and PV are analyzed, including positive and negative reserve. Positive reserve is mainly used by the customer to actively reduce the power consumption for responding to the system scheduling. And negative reserve is used by the

Table 2: The parameters of CPP.

Unit type	Minimum generation /MW	Maximum generation /MW	Climbing rate /MW	Start-down cost/10^3¥/	Start-down time/h	1 stage slope/ (10^3¥/MW)	2 stage slope/ (10^3¥/MW)
TAURUS60	2.5	5.67	3	1.59	2	1.85	2.12
CENTAUR50	2	4.6	2.5	1.06	1.5	1.16	2.38

customer to increase the power consumption for increasing the grid connection of WPP and PV.

Case 4 (DR scenario). Self-scheduling of MECS with PBDR and IBDR: The scenario is mainly used to analyze the synergistic effect between IBDR and PBDR. The parameter settings are the same as Cases 2 and 3.

5.2. Basic Data. To verify the validity and applicability of the proposed model and algorithm, the paper selects IEEE30 bus system as the simulation system. For this, 1×6.5MW wind turbine and 1×5.67 MW CGT were assessed at point 30, 1×4.5MW PV and 1×4.57MW CGT were assessed at point 29, and IBDR and PBDR were assessed at point 27; Figure 3 is the improved IEEE30 bus system structure diagram with MECS. Table 2 is the parameter of CGT. For ease of calculation, linearize the CGT cost function curve into two stages with reference to literature [4]. Table 1 is the parameter of CGT.

According to literature [25], select demand load data in typical load day. To encourage users to participate in system optimization scheduling, set the user electricity price as 0.59¥/kW h before PBDR. With reference to literature [26], the electricity demand price is introduced. Assume the price in the flat period remains unchanged, the price in the peak period is increased by 30%, and the price in the valley period is reduced by 50%. At the same time, when IBDR provides positive output power, it indicates that the power consumption is reduced, and the energy price is set as 0.65¥/kW h. When IBDR provides negative output power, it indicates that the power consumption is increased, and the preferential price is 0.35¥/kW h. To avoid the large load fluctuation causing by peak-valley upside down, this paper sets that the load change produced by PBDR does not exceed 15% of the original load, and the output of IBDR participating into MECS scheduling does not exceed ±1.5MW [2]. Table 3 shows the basic parameters of IBDR and PBDR.

Set WPP, PV, and CGT grid-connected electricity prices as 0.56¥/kW h, 0.5¥/kW h, and 0.8¥/kW h, respectively. The price of MECS purchasing power from the public grid is 0.95¥/kW h. Assume the cut-in, rated and cut-out wind velocity of WPP are 2.8m/s, 12.5m/s and 22.8m/, the shape coefficient $\varphi = 2$, and the scale coefficient $\vartheta = 2\overline{v}/\sqrt{\pi}$ [5]. According to literature [26], the illumination intensity parameters ξ and ψ are 0.3 and 8.54. When PDFs of wind velocity, radiation intensity, and demand load are gain, 50 groups of simulation scenarios would be generated and 10 typical scenarios are gotten by the proposed scenario simulation method. Scenario with the maximum probability is taken as the input data. Figure 4 is the simulation scenario of WPP, PV, and demand load.

After inputting the above basic data, the model is solved by the GAMS software using CPLEX 11.0 linear solver from ILOG-solver [26]. The CPU time is required for solving the problem for different case studies with an idea pad450 series laptop computer powered by core T6500 processor and 4 GB of RAM. The time for solving the model under four cases is less than 20s. When the optimization is MILP, the GAMs software could get a satisfactory solution quickly. Figure 5 is the optimization flowchart for MECS scheduling model.

5.3. Result Analysis

5.3.1. Self-Scheduling Results in Case 1. This scenario is used as the basic scenario and is mainly used to analyze the validity of the proposed multiobjective algorithm. Firstly, each objective function is used as the system optimization objective, and the model is solved to obtain the MECS scheduling results under different objective functions. The time for solving the model is less than 95s by the proposed algorithm. The operation speed is fast and convergence effect is good. Figure 6 shows the self-scheduling results of MECS in different objective functions.

Then, according to Figure 6, when aiming at the maximum economic benefit objective, MECS will rationally arrange different generator sets to generate electricity based on the load demand, and the economic benefit value is 108669.28 ¥. When aiming at the minimum abandoned energy objective, the grid-connected electricity of WPP and PV is 91.947 MW h and 44.068 MW h, respectively, and the minimum abandoned energy is 10.238 MW h. When aiming at the minimum system volatility objective, the grid-connected electricity of WPP and PV will be reduced for minimizing the system operation risk, and the maximum abandoned energy amount is 17.55 MW h and the minimum load fluctuation reaches 9.58 MW h. Then, the payoff table of MECS could be obtained. Table 4 is the payoff table of objective function.

Thirdly, according to Table 4, it can be determined that the maximum values of the objective functions f_1, f_2, and f_3 are, respectively, 108669.28 ¥, 17.55 MW h, and 10.15 MW, and the minimum values are, respectively, 105398.54 ¥, 10.238 MW h, and 9.58 MW. Using the proposed algorithm to solve the objective function weight system, the weights of the three objective functions can be obtained as 0.364, 0.340, and 0.296, respectively. Then, using (47) to solve the system scheduling optimization result under weighted integrated single objective, the optimal values for f_1, f_2, and f_3 are 108009.30 ¥, 11.620 MW h, and 9.74 MW, respectively. Figure 7 is the self-scheduling result of MECS in Case 1.

Finally, according to Figure 7, we can see that in order to take into account the system operation economic benefit,

Table 3: The basic parameters of PBDR and IBDR.

		After PBDR			IBDR	
	Before PBDR	Peak load period	Valley load period	Float load period	+	-
Time divide		9:00-11:00; 18:00-24:00	0:00-8:00	12:00-17:00		
Power price (¥/kW·h)	0.59	0.767	0.295	0.59	0.65	0.35

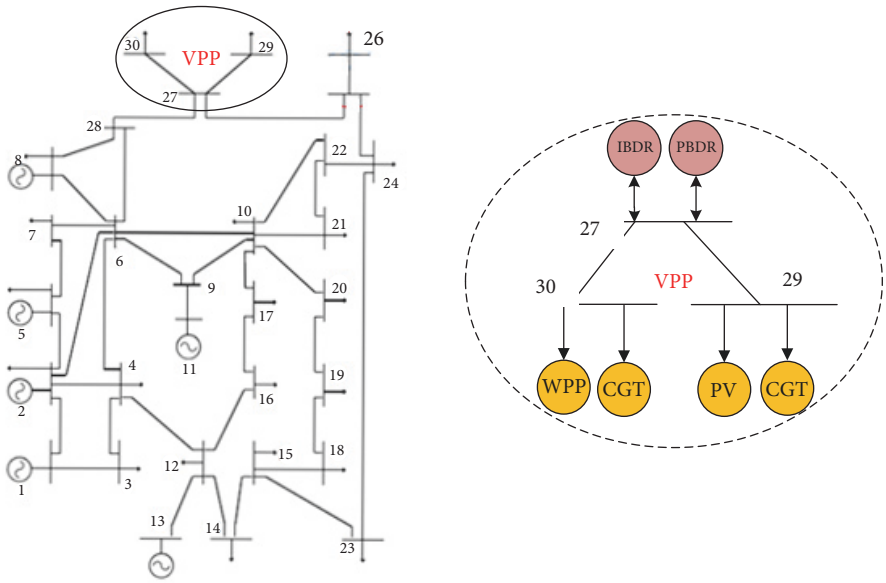

Figure 3: The improved IEEE30 system structure diagram with MECS.

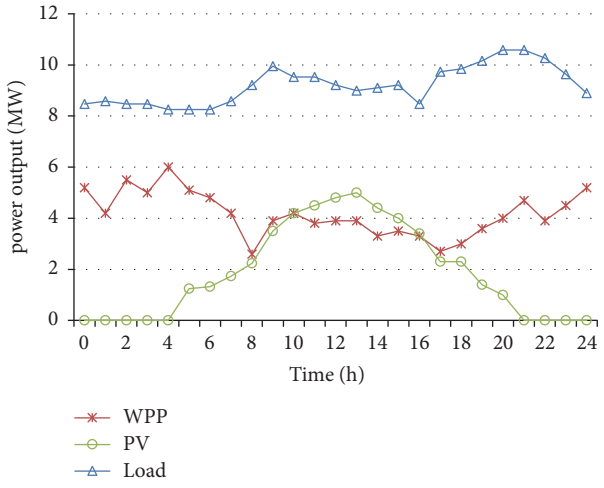

Figure 4: Simulation scenario of WPP, PV, and demand load.

abandoned energy, and risk level, MECS will priorly invoke WPP and PV to meet the user load demands, and the WPP an PV power generation is 90.957 MW h and 43.594 MW h, respectively. At the same time, CGT is used to provide peaking services for WPP and PV with the total power generation of 91.86 MW h. MECS will use CGT with high peaking capacity to meet WPP and PV peaking demands, especially during the load peak period. The total operating economic benefit is 108009.25 ¥. In general, the proposed algorithm can be used to solve the multiobjective optimization model. Under the weighted integrated optimal model, the scheduling results can better consider the demands from different aspects and have a better balance.

5.3.2. Self-Scheduling Results Case 2. The scenario is mainly used to analyze the optimization effect of PBDR on MECS operation, especially the smooth effect of PBDR on the load curve, so as to increase the grid connection capacity of WPP and PV. In Case 2, the optimal values of f_1, f_2, and f_3 for MECS operation are, respectively, 109501.8 ¥, 7.31 MW h, and 9.80 MW, and the power generation capacity of WPP and PV is, respectively, 93.92 MW h and 45.02MW h. Figure 8 is the self-scheduling of MECS in Case 2.

According to Figure 8, the load demand curve is gentler after PBDR, and the grid connection capacity for WPP and PV improves. The total abandoned energy capacity of WPP and PV is 7.31MW h. Compared with Figure 7, PBDR makes the load curve gentler during the peak period. Besides, the grid connection capacity of WPP and PV increases, and the grid-connected electricity is 40.128 MW h and 16.875 MW h, respectively. Figure 9 is the load demand before and after PBDR.

According to Figure 9, PBDR can smooth the load demand curve, which makes the peak load decrease from 10.59 MW h to 10.16 MW h and the valley load increase from

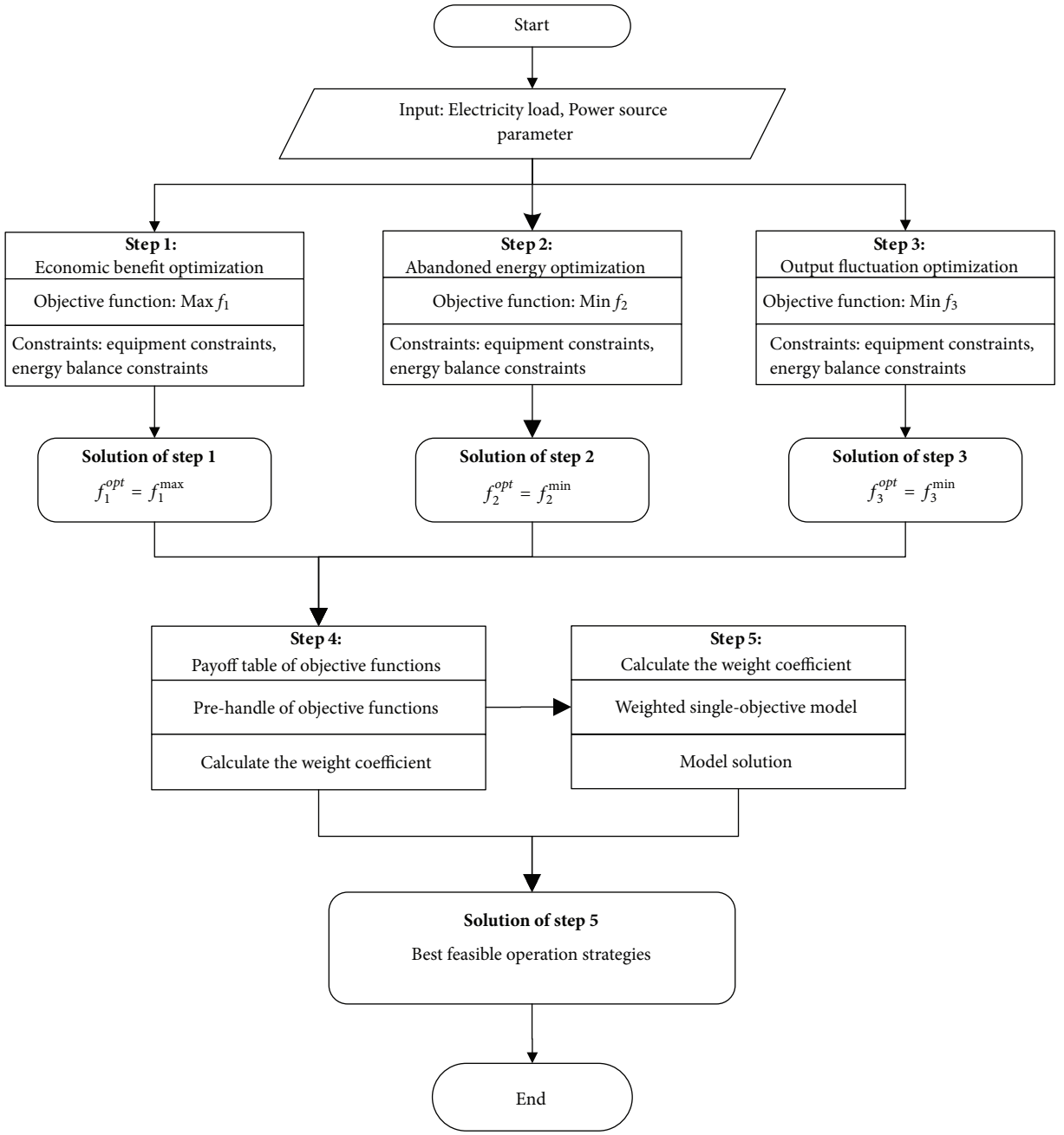

Figure 5: Multiobjective joint optimization flowchart of MECS system.

Table 4: The payoff table of objective function.

	f_1/¥	f_2/MW•h	f_3/MW	Power output/MW·h		
				WPP	PV	CGT
f_1	*108669.28*	14.624	9.85	88.98	42.65	94.94
f_2	106677.75	*10.238*	10.15	91.95	44.07	90.28
f_3	105398.54	17.550	*9.58*	87.00	41.70	98.28
Max	108669.28	17.55	10.15	91.95	44.07	98.28
Min	105398.54	10.238	9.58	87.00	41.70	90.28

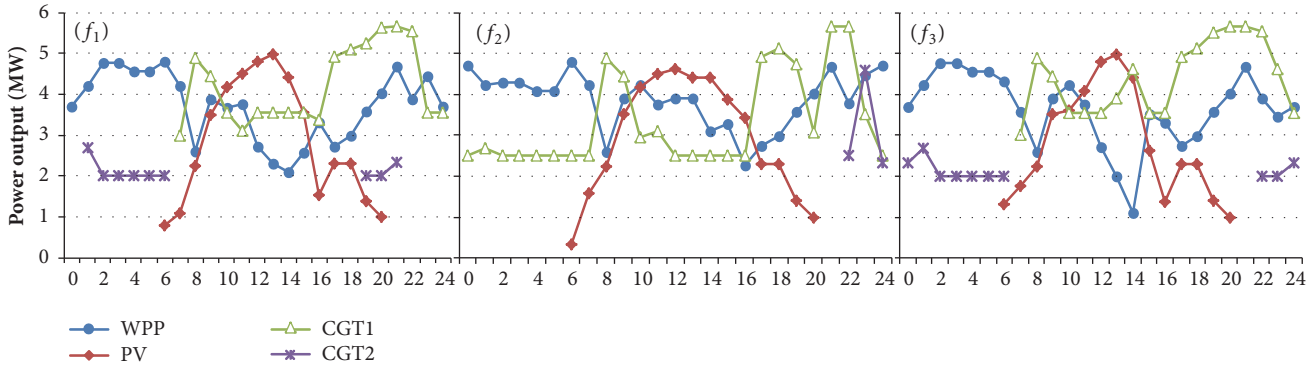

Figure 6: The self-scheduling results of MECS in different objective functions.

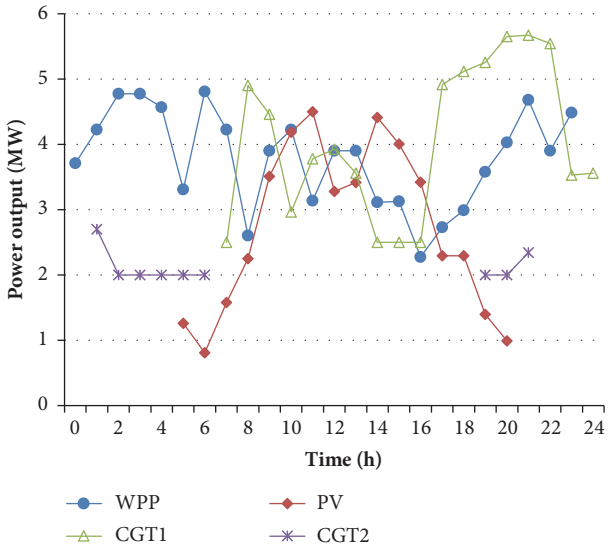

Figure 7: The self-scheduling result of MECS in Case 1.

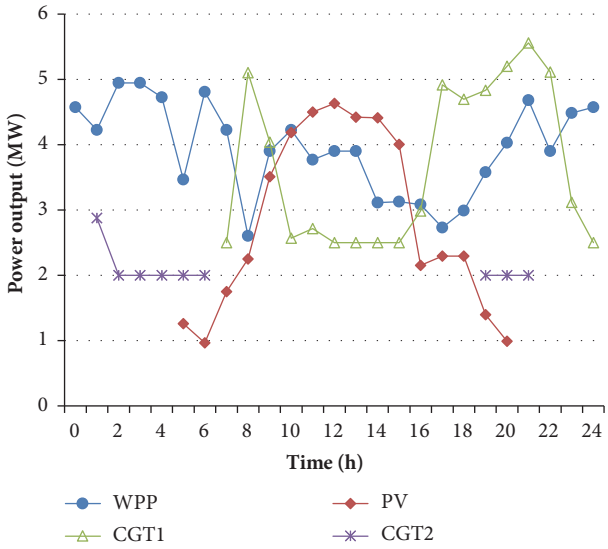

Figure 8: The self-scheduling result of MECS in Case 2.

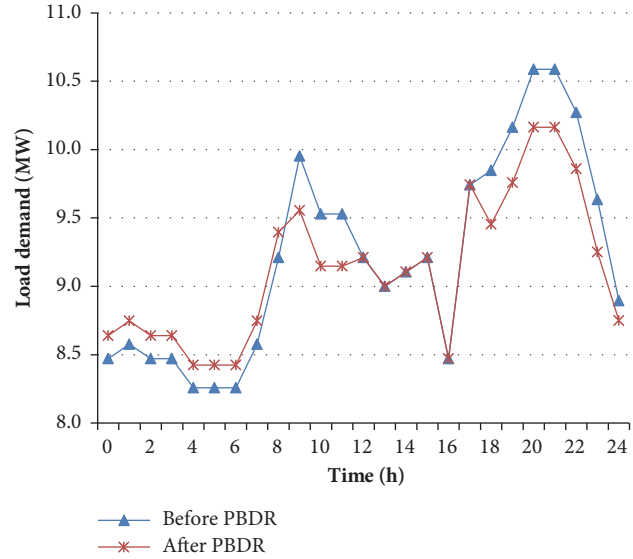

Figure 9: The load demand before and after PBDR.

8.26 MW h to 8.42 MW h. And the peak-to-valley ratio also decreases from 1.28 to 1.21, which provides more capacity for the grid connection of WPP and PV. However, the increase in the grid connection of WPP and PV does not bring in more peaking demand of CGT. Correspondingly, the total power output of CGT is 84.71MW h in Case 2, which is 7.15MW·h lower than that in Case 1. In general, PBDR can optimize MECS scheduling operation by optimizing the user power consumption behavior.

5.3.3. Self-Scheduling Results Case 3. The scenario is mainly used to analyze the optimization effect of IBDR on MECS operation, especially the peaking service capability provided by IBDR for WPP and PV. In Case 3, the optimal values for f_1, f_2, and f_3 of MECS operation are 109563.5 ¥, 8.77 MW h, and 7.81 MW, respectively. And the grid-connected electricity for WPP and PV is 92.93 MW h and 44.54 MW h, respectively. The grid-connected electricity of CGT is 89.89 MW h. Figure 10 is the self-scheduling result of MECS in Case 3.

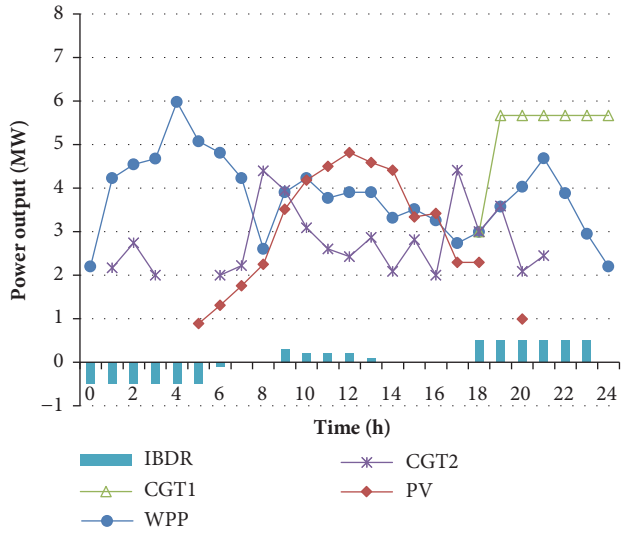

Figure 10: The self-scheduling result of MECS in Case 3.

According to Figure 10, when the IBDR is integrated into MECS, the peaking services of WPP and PV can be provided jointly by CGT and IBDR. The grid-connected electricity of WPP and PV increases significantly, and the abandoned energy amount decreases from 11.70 MW h in Case 1 to 8.77 MW h in Case 3. Compared with Figure 7, IBDR provides more capacity for the grid connection of WPP and PV by using price concessions to increase valley load. And the grid-connected electricity of WPP and PV increases to 38.327 MW h and 6.2 MW h in Case 3. Then, as IBDR provides peaking services for WPP and PV, the power output of CGT is significantly reduced from 91.86 MW h to 89.89 MW h. Further, the output results of IBDR under different peaking prices are analyzed. Figure 11 is the IBDR output under different peaking prices.

According to Figure 11, the peaking price directly affects IBDR output. On the whole, as the peaking price increases, IBDR output also increases accordingly, but it is not a direct positive correlation. When price changes in the range of [-20%, 20%], the rising price will prompt IBDR output to quickly increase. When the price changes outside [-20%, 20%], IBDR output fluctuation range generated by the rising price is also relatively flat, indicating that the callable space for IBDR has basically reached the upper limitation. Therefore, in order to ensure the stable operation of MECS, it is necessary to reasonably set the peaking service price according to the actual situation.

5.3.4. Self-Scheduling Results Case 4. The scenario is mainly used to analyze the synergistic optimization effects between PBDR and IBDR, which is the interaction between IBDR internal peaking capability and the PBDR external grid connection capacity enhancing ability. The optimal values of f_1, f_2, and f_3 for MECS operation are 110627.25 ¥, 5.85 MW h, and 8.06 MW, respectively. The total grid-connected electricity of WPP and PV is, respectively, 94.91 MW h and 45.49 MW h, and the power generation of CGT is 85.46 MW h. Figure 12 is the self-scheduling result of MECS in Case 4.

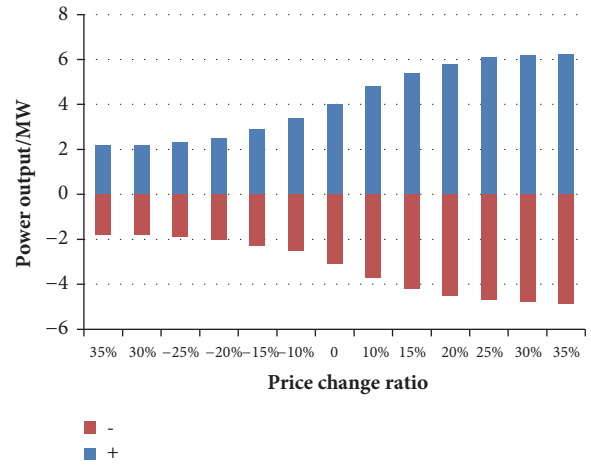

Figure 11: The IBDR output under different peaking prices.

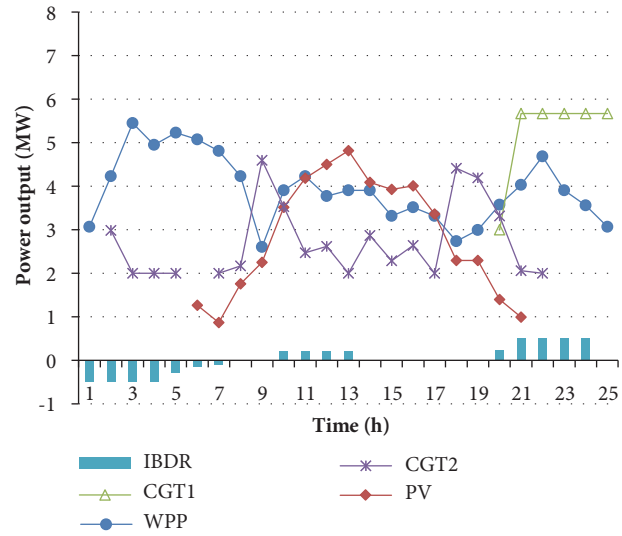

Figure 12: The self-scheduling result of MECS in Case 4.

According to Figure 12, after simultaneously introducing PBDR and IBDR, the grid connection capacity of WPP and PV improves, and the abandoned energy reaches the lowest value, which is 5.85 MW h. Compared to Case 1, the abandoned energy decreases from 11.70 MW h to 5.85 MW h. The increase in grid-connected electricity of WPP and PV also adds the overall system operation economic benefit, from 108009.25 ¥ to 110627.25 ¥, while the load fluctuation decreases from 9.03 MW to 8.06 MW. Therefore, after the joint introduction of IBDR and PBDR, the synergetic optimization effect can be achieved, and both the operation benefit and the abandoned energy are optimal. However, it is worth noting that 8.06 MW of load fluctuation has not reached the minimum. This is because IBDR and CGT provide sufficient peaking service for WPP and PV; thus the grid-connected electricity of WPP and PV reaches the maximum, which also increases the system load fluctuation correspondingly. Figure 13 is the power output of MECS in different cases.

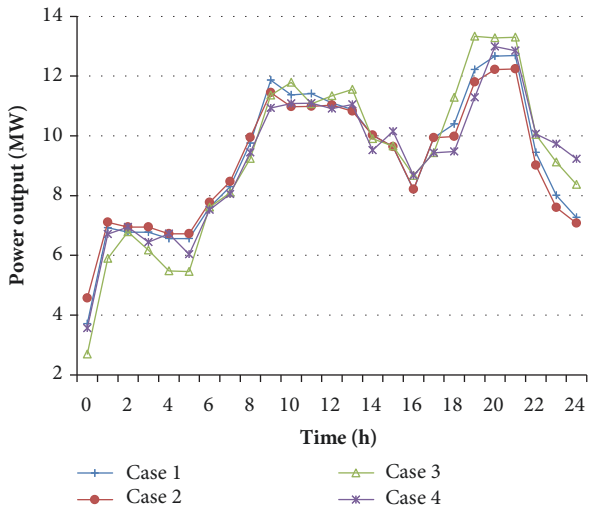

Figure 13: The power output of MECS in different cases.

Then, the power output of MECS in different cases is comparatively analyzed. According to Figure 13, IBDR and PBDR can smooth the power output curve of MECS. Compared with Case 1, the load curve becomes gentler after the introduction of PBDR in Case 2. Correspondingly, the MECS output curve also becomes flat, and the output increases during the valley period and the output decreases during the peak period. Compared with Case 1, after the introduction of IBDR in Case 3, the MECS can reduce the power consumption by invoking users during the peak period and provide positive output, making MECS output significantly increase. And during the valley period, the MECS can increase the power consumption by invoking users and provide negative output, making MECS output decrease. When IBDR and PBDR are simultaneously introduced in Case 4, MECS can use PBDR and IBDR at the same time to achieve the synergetic optimization effect, and the system scheduling result is optimal. Table 5 shows the scheduling results of MECS in different cases.

Finally, according to Table 5, PBDR and IBDR have significant synergistic optimization effect and can achieve maximum grid connection of WPP and PV and the minimum abandoned energy. DR fully invokes the users to participate in the system operation, making the load curve become gentler and the peak-to-valley ratio decrease from 1.28 in Case 1 to 1.19 in Case 4. Based on the PBDR and IBDR participating in the system scheduling output power, it can be seen that output power has decreased in Case 4 compared with IBDR in Case 3 and PBDR in Case 2. The implementation of PBDR can optimize MECS operation externally, while IBDR can optimize the MECS operation internally. It can achieve the optimal scheduling of MECS and maximize the utilization of WPP and PV in Case 4. Therefore, decision makers should coordinate use of PBDR and IBDR to promote the grid connection of clean energy.

6. Conclusions

In this paper, WPP, PV, CGT, and IBDR are aggregated into MECS. PBDR is implemented for optimizing MECS operation scheduling. Then, the maximum economic benefit, the minimum abandoned energy, and the minimum risk level are taken as the objective functions for constructing a multiobjective model for MECS scheduling considering system operation constraints. Thirdly, the payoff table of MECS scheduling under signal objective function is calculated for solving the weight coefficients of different objective functions by entropy method and converting the multiobjective model into the single objective model with the weight coefficients. Finally, the improved IEEE 30 bus system is taken as the simulation system, and the simulation result shows the following.

(1) The MECS can fully utilize the complementarity of different power sources. WPP and PV are used to meet the end-user load demands. IBDR can utilize user side resource to respond to the system scheduling and provide peaking services for WPP and PV. When the peaking capacity is insufficient or the WPP and PV are insufficient, the CGT can be invoked to meet the load demand. In general, making full use of the coupled operation of WPP, PV, CGT, and IBDR is conducive to play the complementary features of different power sources and then realize the system overall optimized operation.

(2) The proposed algorithm can be used to solve the MECS multiobjective scheduling optimization model, while the system scheduling results in the comprehensive optimal mode can take into account different appeal. The total system benefit reaches a maximum of 108669.28 ¥ in the optimal economic benefit mode, while the abandoned energy reached a minimum of 10.238 MW h in the minimum abandoned energy mode, and the system load fluctuation reaches a minimum of 9.58 MW in the minimum risk mode. In the comprehensive optimal model, the total system benefit, abandoned energy, and load fluctuation are 108009.30 ¥, 11.62 MW h, and 9.74 MW, respectively. Therefore, the proposed MECS scheduling model and solution algorithm can provide the decision basis for the decision makers according to the actual situation.

(3) PBDR and IBDR have significant synergistic optimization effects, which can provide greater capacity for the grid connection of WPP and PV. PBDR can achieve the peak load shifting in the load curve, but the peaking capability is weaker than IBDR. When PBDR is introduced separately, the peak-to-valley ratio of the load curve is 1.21, and the abandoned energy is 7.31 MW h. When IBDR is introduced separately, the peak-to-valley ratio of the load curve is 1.24, and the abandoned energy is 8.77 MW h. When both are introduced, the peak-to-valley ratio of the load curve is 1.19, and the abandoned energy is 5.85 MW h. In short, decision makers should coordinate use of PBDR and IBDR to promote the grid connection of clean energy based on actual conditions.

Data Availability

All basic data used to support the findings of this study are included within the article.

Conflicts of Interest

The authors declare that there are no conflicts of interest regarding the publication of this paper.

Table 5: Scheduling results of MECS in different cases.

	Object function value			VPP power output/MW·h			DR/MW·h					Peak-to-valley ratio
	f_1 /10^3¥	f_2 /MW·h	f_3 /MW	WPP	PV	CGT	IBDR		PBDR			
							+	-	peak	flat	valley	
Case 1	108.01	11.70	9.03	90.96	43.59	91.86	-	-	-	-	-	1.28
Case 2	109.50	7.31	9.80	93.92	45.02	84.71	-	-	-2.73	0.45	1.53	1.21
Case 3	109.56	8.77	7.81	92.93	44.54	89.89	4	-3.1	-		-	1.24
Case 4	110.63	5.85	8.06	94.91	45.49	83.46	3.6	-2.54	-2.45	0.25	1.28	1.19

Acknowledgments

The work is partially supported by Science Foundation of China University of Petroleum, Beijing (no. ZX20170256), and supported by Beijing Social Science Fund.

References

[1] http://guangfu.bjx.com.cn/news/20180213/880991.shtml.

[2] Z. Tan, G. Wang, L. Ju, Q. Tan, and W. Yang, "Application of CVaR risk aversion approach in the dynamical scheduling optimization model for virtual power plant connected with wind-photovoltaic-energy storage system with uncertainties and demand response," *Energy*, vol. 124, pp. 198–213, 2017.

[3] G. Boukettaya and L. Krichen, "A dynamic power management strategy of a grid connected hybrid generation system using wind, photovoltaic and Flywheel Energy Storage System in residential applications," *Energy*, vol. 71, pp. 148–159, 2014.

[4] Z.-F. Tan, L.-W. Ju, H.-H. Li, J.-Y. Li, and H.-J. Zhang, "A two-stage scheduling optimization model and solution algorithm for wind power and energy storage system considering uncertainty and demand response," *International Journal of Electrical Power & Energy Systems*, vol. 63, pp. 1057–1069, 2014.

[5] L. Ju, Z. Tan, J. Yuan, Q. Tan, H. Li, and F. Dong, "A bi-level stochastic scheduling optimization model for a virtual power plant connected to a wind-photovoltaic-energy storage system considering the uncertainty and demand response," *Applied Energy*, vol. 171, pp. 184–199, 2016.

[6] J. He, C. Deng, Q. Xu, C. Liu, and H. Pan, "Optimal configuration of distributed generation system containing wind PV battery power sources based on equivalent credible capacity theory," *Dianwang Jishu/Power System Technology*, vol. 37, no. 12, pp. 3317–3324, 2013.

[7] M. Ding, B. Wang, and B. Zhao, "Configuration Optimization of Capacity of Standalone PV-Wind-Diesel-Battery Hybrid Microgrid," *Power System Technology*, vol. 37, no. 3, pp. 575–581, 2013.

[8] G. Mavromatidis, K. Orehounig, and J. Carmeliet, "Uncertainty and global sensitivity analysis for the optimal design of distributed energy systems," *Applied Energy*, vol. 214, pp. 219–238, 2018.

[9] Z. Liu, Y. Chen, R. Zhuo, and H. Jia, "Energy storage capacity optimization for autonomy microgrid considering CHP and EV scheduling," *Applied Energy*, vol. 210, pp. 1113–1125, 2018.

[10] A. Zidan, H. A. Gabbar, and A. Eldessouky, "Optimal planning of combined heat and power systems within microgrids," *Energy*, vol. 93, pp. 235–244, 2015.

[11] F. Xu, Y. Min, and L. Chen, "Combined electricity-heat operation system containing large capacity thermal energy storage," in *Proceedings of the CSEE*, vol. 34, pp. 5063–5072, 2014.

[12] G. R. Huang, W. J. Liu, F. S. Wen et al., "Collaborative planning of intergrated electricity and natural gas energy systems with power-to-gas stations," *Electric Power Construction*, vol. 37, no. 9, pp. 1–13, 2016.

[13] H. Pandžić, I. Kuzle, and T. Capuder, "Virtual power plant mid-term dispatch optimization," *Applied Energy*, vol. 101, pp. 134–141, 2013.

[14] P. Duan, J. Q. Zhu, M. B. Liu et al., "Optimal Dispatch of Virtual Power Plant Based on Bi-Level Fuzzy Chance Constrained Programming," *Transactions of China electrotechnical Society*, vol. 31, no. 09, pp. 58–67, 2016.

[15] M. J. Kasaei, M. Gandomkar, and J. Nikoukar, "Optimal management of renewable energy sources by virtual power plant," *Journal of Renewable Energy*, vol. 114, pp. 1180–1188, 2017.

[16] J. Zhu, P. Duan, and M. Liu, "Electric real-time balance dispatch via bi-level coordination of source-grid-load of power system with risk," *Zhongguo Dianji Gongcheng Xuebao/Proceedings of the Chinese Society of Electrical Engineering*, vol. 35, no. 13, pp. 3239–3247, 2015.

[17] Z. Hu, H. Ding, and T. Kong, "A joint daily operational optimization model for wind power and pumped-storage plant," *Automation of Electric Power Systems*, vol. 36, no. 2, pp. 36–57, 2012.

[18] J. H. Drake, L. K. Kirchmayer, R. B. Mayall, and H. Wood, "Optimum Operation of a Hydrothermal System," *Transactions of the American Institute of Electrical Engineers. Part III: Power Apparatus and Systems*, vol. 81, no. 3, pp. 242–248, 1962.

[19] Z. Soltani, M. Ghaljehei, G. B. Gharehpetian et al., "ntegration of smart grid technologies in stochastic multi-objective unit commitment: An economic emission analysis," *International Journal of Electrical Power & Energy Systems*, vol. 100, pp. 565–590, 2018.

[20] R. Q. Wang, C. H. Zhang, and K. Li, "Multi-objective genetic algorithm based on improved chaotic optimization," *Kongzhi yu Juece/Control and Decision*, vol. 26, no. 9, pp. 1391–1397, 2011.

[21] M. Nemati, M. Braun, and S. Tenbohlen, "Optimization of unit commitment and economic dispatch in microgrids based on genetic algorithm and mixed integer linear programming," *Applied Energy*, vol. 210, pp. 944–963, 2018.

[22] J. Chen, X. Yang, and L. Zhu, "Microgrid Multi-objective Economic Dispatch Optimization [J]," in *Proceedings of the CSEE*, vol. 33, pp. 57–66, 2013.

[23] C. Deng, L. Ju, J. Liu, and Z. Tan, "Stochastic scheduling multi-objective optimization model for hydro-thermal power systems based on fuzzy CVaR theory," *Dianwang Jishu/Power System Technology*, vol. 40, no. 5, pp. 1447–1454, 2016.

[24] L. Ju, Z. Tan, H. Li, Q. Tan, X. Yu, and X. Song, "Multi-objective operation optimization and evaluation model for CCHP and renewable energy based hybrid energy system driven by distributed energy resources in China," *Energy*, vol. 111, pp. 322–340, 2016.

[25] L. Ju, H. Li, J. Zhao, K. Chen, Q. Tan, and Z. Tan, "Multi-objective stochastic scheduling optimization model for connecting a virtual power plant to wind-photovoltaic-electric vehicles considering uncertainties and demand response," *Energy Conversion and Management*, vol. 128, pp. 160–177, 2016.

[26] Z. Tan, L. Ju, B. Reed et al., "The optimization model for multi-type customers assisting wind power consumptive considering uncertainty and demand response based on robust stochastic theory," *Energy Conversion and Management*, vol. 105, pp. 1070–1081, 2015.